INT. J. NUM. METH. HEAT FLUID FLOW, VOL. 2, 379–390 (1992)

FULLY DEVELOPED LAMINAR FLUID FLOW AND HEAT TRANSFER IN A STREAMWISE-PERIODIC CORRUGATED DUCT WITH CONSTANT CROSS-SECTIONAL AREA

BIJAN FARHANIEH AND BENGT SUNDÉN

Department of Thermo- and Fluid Dynamics, Chalmers University of Technology, S-412 96 Göteborg, Sweden

ABSTRACT

Laminar fully developed periodic heat transfer and fluid flow characteristics in corrugated two-dimensional ducts with constant cross-sectional area are numerically investigated. The governing equations are solved numerically by a finite-volume method for elliptic flows in complex geometries using colocated variables and Cartesian velocity components. The results were obtained for a uniform wall temperature for two inclination angles ϕ and three duct aspect ratios (H/L) and for Reynolds number ranging from 30 to 1200. The plot of the velocity vectors show a complex flow pattern. Unexpected high enhancement of the average Nusselt number was observed at low Reynolds number for $H/L = 1/2$ and $1/3$. A moderate increase in Nusselt number was obtained as Reynolds number was increased further.

KEY WORDS Corrugated ducts Laminar fluid flow Finite volume method

NOMENCLATURE

A	dimensionless per-cycle heat transfer surface area
A'	dimensionless flow cross-sectional area
B	dimensionless pressure drop
c_p	specific heat
D_h	hydraulic diameter ($= 2H$)
$\mathrm{d}A_c$	incremental flow cross-sectional area
H	height of the duct
h	heat transfer coefficient
k	thermal conductivity of the fluid
L	streamwise length of a module
$\dot{m}$	mass flow rate
Nu	average Nusselt number
Nu_x	circumferential local Nusselt number
P	dimensionless periodic pressure
p	pressure
p^*	periodic pressure
Pr	Prandtl number
$\dot{Q}$	per-cycle wall heat transfer rate
Re	Reynolds number
S	top length of the cavity
S_Φ	source term in general equation
T	temperature
U	dimensionless axial velocity
u_i	velocity components
u_m	mean velocity
V	dimensionless velocity in y-direction
X	dimensionless streamwise coordinate
x	streamwise coordinate
Y	dimensionless coordinate
y	coordinate
β	non-periodic pressure gradient
γ	bulk-to-wall temperature ratio
ΔP	per-cycle pressure drop in corrugated duct
ΔP_0	pressure drop in parallel plate duct
Δt_{wb}	average wall-to-bulk temperature difference
η	distance normal to the wall
Θ	dimensionless temperature
λ	bulk-temperature-gradient parameter
μ	dynamic viscosity
ν	kinematic viscosity
ρ	density
ϕ	inclination angle

0961–5539/92/050379–12$2.00

Received March 1992
Revised June 1992

INTRODUCTION

An effective way to reduce heat exchanger costs is to employ more compact surfaces. This causes improvements in both the cost per unit area and heat transfer flux per unit temperature difference. A variety of channels with different geometries have been utilized for internal flow forced convection heat transfer studies. Numerical as well as experimental laminar flow results for some of these channels are available in the open literature, e.g. see Shah and Bhatti[1]. An alternative way of achieving higher convective heat transfer is to use corrugated channels. Some experimental results are available in the literature, see Webb[2]. The numerical approach for solution of such problems is usually based upon the assumption that the duct is long and consists of many identical modules in the streamwise direction where the fully developed velocity field repeats itself in a cyclic manner. This assumption enables us to ignore the influence of the entrance and exit regions and confine the calculation domain to cover only one of the modules.

The methodology for fully developed solutions of this kind of problems was presented by Patankar *et al.*[3]. This methodology has been used by Sparrow and Prata[4,5] to study laminar flow and heat transfer in a periodically converging-diverging tube and in an annulus of periodically varying cross section. Rowley and Patankar[6] applied this method in their study of tubes with internal circumferential fins. Faghri and Asako[7,8], Webb and Ramadhyani[9] and Sunden and Trollheden[10] have also successfully adopted this method in their studies of various ducts with streamwise-periodic variations of cross-sectional areas. Through these studies it has been shown that higher convective heat transfer coefficients can be achieved by employment of corrugated channels but the pressure drop is also increased.

In an earlier paper by Farhanieh and Sunden[11], the fully developed periodic laminar flow and heat transfer in a duct having periodically varying cross-sectional area with converging-diverging cavities were considered. In this paper, the cross-sectional area of the corrugated duct is constant along the main flow direction but the corrugations on the top and bottom walls are in phase.

The numerical method used is a finite-volume method for elliptic flows in non-orthogonal coordinates which utilizes colocated variables and Cartesian velocity components. The details of the method are documented in a report by Davidson and Farhanieh[12] and have also been presented in a previous paper by Farhanieh and Sunden[13]. Numerical solutions were carried out for a uniform wall temperature boundary condition at two values of the inclination angle ϕ, and three values of the cycle aspect ratio ($= H/L$). The computations were performed in the Reynolds number (based on hydraulic diameter) range 30 to 1200 and for $Pr = 0.72$ corresponding to air. Nusselt numbers and pressure drop data as well as, velocity vectors are presented.

PROBLEM FORMULATION

The duct considered is presented schematically in *Figure 1*. The oblique walls are positioned at an angle ϕ to the main flow direction. The geometry of the channel can be specified by the periodic axial full length L, the height H, lengths a_1, a_2 and S, and inclination angle ϕ. The dimensions of the duct are: $a_1 = 0.1L$, $a_2 = 0.25L$ and $S = 0.3L$. The values of 15° and 45° were chosen for the corrugation inclination angle ϕ. The ratio H/L is varied.

The heat transfer and fluid flow characteristics for laminar, incompressible, forced convection along the cycle length are to be determined. The walls of the duct are kept at a uniform temperature. The axial velocity is in the x-direction.

GOVERNING EQUATIONS

The governing equations are the continuity, momentum and energy equations. Consideration is given to fully developed periodic laminar flow. The flow is studied under the following

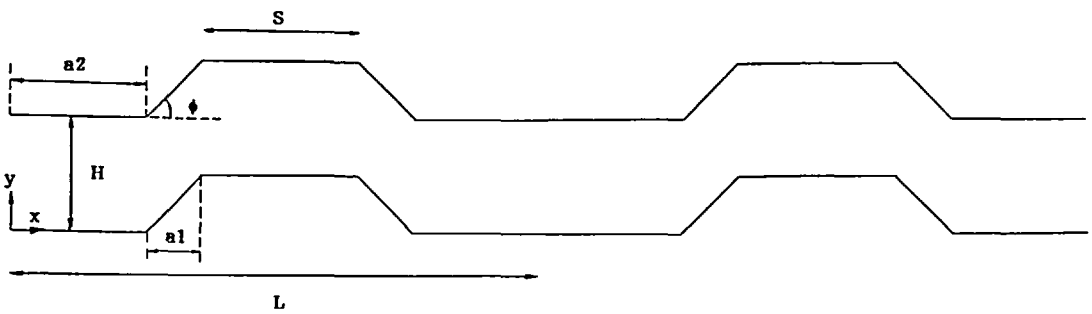

Figure 1 Schematic diagram of the duct

assumptions: steady state, constant fluid properties, negligible viscous dissipation and no natural convection.

The pressure p, is expressed by:

$$p(x, y) = -\beta x + p^*(x, y) \tag{1}$$

where p^* behaves in a periodic manner from cycle to cycle. In βx, β is a constant representing the non-periodic pressure gradient in the flow direction.

The following dimensionless variables are introduced.

$$X_i = \frac{x_i}{L} \qquad U_i = \frac{u_i L}{\nu} \qquad P = \frac{p^*}{\rho\left(\frac{\nu}{L}\right)^2} \qquad B = \frac{\beta L}{\rho\left(\frac{\nu}{L}\right)^2} \qquad \Theta = \frac{t - t_w}{t_b - t_w}$$

where L and ν are the periodic cycle length and the kinematic viscosity, respectively. Subscript i refers to the x- and y-directions.

The governing equations take the following non-dimensional form in a Cartesian coordinate system.

$$\frac{\partial U}{\partial X} + \frac{\partial V}{\partial Y} = 0 \tag{2}$$

$$U\frac{\partial U}{\partial X} + V\frac{\partial U}{\partial Y} = -\frac{\partial P}{\partial X} + B + \nabla^2 U \tag{3}$$

$$U\frac{\partial V}{\partial X} + V\frac{\partial V}{\partial Y} = -\frac{\partial P}{\partial Y} + \nabla^2 V \tag{4}$$

$$U\frac{\partial \Theta}{\partial X} + V\frac{\partial \Theta}{\partial Y} - \frac{1}{Pr}\nabla^2\Theta = \frac{\sigma}{Pr} \tag{5}$$

where

$$\sigma = \lambda\left(2\frac{\partial \Theta}{\partial X} - PrU\Theta\right) + \Theta\left(\lambda^2 + \frac{\partial \lambda}{\partial X}\right) \tag{6}$$

and

$$\lambda = \frac{\partial(t_b - t_w)}{\partial X}\Big/(t_b - t_w) \tag{7}$$

where σ and λ are periodic parameters for the case of a constant wall temperature and t_b the fluid bulk temperature.

The shape of the non-dimensional temperature profile $\Theta(x, y)$ repeats itself in the fully developed periodic area.

The boundary conditions at the walls are:

$$U = V = 0 \qquad \Theta = 0$$

At the inlet and outlet of the module, conditions of periodicity are imposed, that is

$$\Phi(x, y) = \Phi(x + L, y) \qquad \Phi = U, V, P, \Theta, \lambda$$

Since the convective heat transfer equation contains two unknowns, $\Theta(x, y)$ and $\lambda(x)$, an additional condition is needed to close the problem. The dimensionless temperature Θ must be compatible with the definition of the bulk temperature. In dimensionless form we have:

$$\int \Theta |U| \, dA' = \int |U| \, dA' \tag{8}$$

This equation gives the lacking condition for the dimensionless temperature field. From (8) it is obvious that the bulk temperature used in the definition of Θ is not the real bulk temperature but rather a local reference temperature which takes into account recirculation zones, see also Patankar *et al.*[3].

NUMERICAL SOLUTION PROCEDURE

To extend the capabilities of the finite difference method to deal with complex geometries, a boundary fitted coordinate method is used. The basic idea is to map the complex flow domain in the physical space to a rectangular domain in the computational space by using a curvilinear coordinate transformation. This means that the Cartesian coordinate system x_i in the physical domain is replaced by a general non-orthogonal coordinate system ξ_i.

The momentum equations are solved for the velocity components U and V in the fixed Cartesian directions on a non-staggered grid. All the variables are thus stored at the centre of the control volume. In order to avoid non-physical oscillations in pressure and velocity, the Rhie–Chow interpolation method is used to compute the velocity components at the control volume faces. The pressure–velocity coupling is handled by the SIMPLEC method. The convective terms are treated by the hybrid scheme. TDMA-based algorithms are applied for solving the algebraic equations. Further details are provided in References 12 and 13.

Reynolds number

The Reynolds number is calculated as:

$$Re = \frac{u_m 2H}{\nu} = \frac{2\dot{m}}{\mu} \tag{9}$$

where ν is the kinematic viscosity and μ the dynamic viscosity. The mass flow rate $\dot{m}$ through a module is evaluated by:

$$\dot{m} = \mu \int_0^{H/L} U \, dY \tag{10}$$

The velocity U depends on the dimensionless non-periodic pressure gradient B. Therefore, (9) and (10) provide a relation between the Re and B.

Pressure drop

The per-cycle pressure drop Δp is calculated as:

$$\Delta p = \beta L \tag{11}$$

It is desirable to compare this pressure drop with the corresponding value for a straight parallel plate duct with hydraulic diameter ($D_h = 2H$). From any standard textbook on fluid mechanics, e.g. White[14], the pressure drop Δp (fully developed flow) in a straight parallel plate duct can be found to be:

$$\Delta p_0 = \frac{96}{Re}\frac{L}{2H}\frac{\rho u_m^2}{2} = \beta_0 L \tag{12}$$

From (12) and (9) and using the definition of B, we obtain

$$B_0 = 6Re\left(\frac{L}{H}\right)^3 \tag{13}$$

where subscript (0) refers to the straight parallel plate duct.

For identical mass flows, the Reynolds number of the straight parallel plate duct becomes equal to that of the corrugated duct and the ratio of the per-cycle pressure drops can be expressed as:

$$\frac{\left(\frac{\Delta p}{L}\right)}{\left(\frac{\Delta p}{L}\right)_0} = \frac{B}{6Re}\left(\frac{H}{L}\right)^3 \tag{14}$$

Local Nusselt number

By using the conventional definition of the heat transfer coefficient between the wall and the fluid (Eckert and Drake[15]) we obtain

$$Nu_x = \frac{hD_h}{k} = D_h\left(\frac{\partial\Theta}{\partial\eta}\right)_{w,x} \tag{15}$$

where Nu_x is the local Nusselt number, k the thermal conductivity of the fluid and η the distance perpendicular to the wall.

Overall Nusselt number

The overall heat transfer coefficient h_{av} is defined by an overall heat balance, that is:

$$h_{av} = \frac{\dot{Q}}{A\Delta t_{wb}} \tag{16}$$

The average wall-to-bulk temperature difference is evaluated as:

$$\Delta t_{wb} = \tfrac{1}{2}\{(t_w - t_{b2}) + (t_w - t_{b1})\} \tag{17}$$

and the total heat flux $\dot{Q}$ is given by:

$$\dot{Q} = \dot{m}c_p(t_{b2} - t_{b1}) \tag{18}$$

where $\dot{m}$ is the mass flow rate and c_p is the specific heat of the fluid. Combining (16), (17), (18)

and the definition of the Nusselt number we have:

$$Nu = \frac{(1-\gamma)}{(1+\gamma)}\frac{H}{A} PrRe \tag{19}$$

where γ is defined as:

$$\gamma = \frac{(t_w - t_{b2})}{(t_w - t_{b1})} \tag{20}$$

The quantity γ is obtained by integrating (7) along the cycle length.

SAMPLE CALCULATIONS

The Prandtl number was set equal to 0.72 and Reynolds number was varied from 30 to 1200 by choosing appropriate values of the per-cycle pressure gradient, B.

Convergence

The computations were terminated when the sum of absolute residuals normalized by the inflow fluxes were below 10^{-4} for all the variables. To achieve convergence in the solution, under-relaxation factors of 0.7 and 0.4 were chosen for the velocities and pressure correction, respectively. About 1000 to 4000 iterations, depending on the Reynolds number and geometrical parameters, were required to obtain a converged solution for the velocity field. The temperature field, which was also solved iteratively (under-relaxation factor 0.8), converged within a few hundred iterations if a known velocity field was used.

Grid size effects and numerical accuracy

The grid points are distributed in a non-uniform manner with higher concentration of grid points close to the walls. Each control volume contains one node at its centre but the boundary adjacent volumes contain two nodes. Typical grids are shown in *Figure 2a* and a principal sketch of the employed grid close to the walls is provided in *Figure 2b*.

Accuracy tests were performed particularly on the effect of the mesh on the solution. The pressure gradient B was prescribed. Since the Reynolds number Re and the per-cycle pressure gradient B are linked to each other through (9) and (10) a grid size effect will also appear as an influence on the Reynolds number. Comparisons of the Reynolds number and the Nusselt numbers for $\phi = 45°$ and $H/L = 1/5$ under various grid sizes were made and are listed in *Table 1*. Between the finest (112 × 46) and coarsest (82 × 38) grids the Reynolds number differs by 5.9% and the Nusselt number differs by 2.8%. In order to keep a moderate computer cost, the computations were performed with 112 × 38 grid points for module aspect ratio 1/5. The test results for this grid deviate from those of the finest grid by 0.1% in the Reynolds number and by 0.66% in the Nusselt number. In the same manner 112 × 46 and 112 × 56 grid points were chosen for the module aspect ratio 1/3 and 1/2, respectively. The test results for $\phi = 15°$ and $H/L = 1/2$ are presented in *Table 2*. The differences between the results are almost negligible. Fully developed flow and heat transfer between parallel plates were also calculated. The computed results agreed well with the analytical results $Nu = 7.54$ and friction factor $96/Re$. The maximum deviations were 0.8% and 0.9%, respectively.

From what has been stated above it is reasonable to assume that the calculated Nusselt numbers are accurate within a few per cent.

To further assess the accuracy of the computational technique, calculations have previously been carried out for various ducts for which analytical and experimental data are available. The

Table 1 Investigation of grid size effect on Nusselt number and Reynolds number for $H/L = 1/5$ and $\phi = 45°$

Grid size	*Re*	*Nu*
82 × 38	381.217	10.033
102 × 38	399.511	9.909
112 × 38	404.620	9.820
112 × 30	407.501	10.055
112 × 46	405.047	9.756

Table 2 Grid size effect on Nusselt number and Reynolds number for $H/L = 1/2$ and $\phi = 15°$

Grid size	*Re*	*Nu*
102 × 46	98.254	15.484
112 × 37	99.593	15.346
112 × 46	99.508	15.346
112 × 56	99.493	15.345

comparison of the Nusselt number and friction factor in fully developed laminar flow in parallel plate ducts agreed well with the analytical results (within 0.17% and 0.32%, respectively) obtained by Shah. The reader is referred to Farhanieh and Sunden[13] for details.

Additional confidence was gained by computing the heat transfer and fluid flow in a channel with a grooved wall and comparing the results with the experimental results of Herman and Mayinger[16]. The numerical results were in good agreement with the experimental results. This latter investigation will be reported elsewhere.

All calculations were carried out on a DEC 3100 work-station.

RESULTS AND DISCUSSION

Flow field

The velocity vectors of the flow through the duct at different locations along the module length are plotted and presented in *Figure 3* for $\phi = 45°$ and module aspect ratio 1/5 for four different Reynolds number. These Figures give a qualitative understanding of the fluid flow pattern in the duct under consideration. At low Reynolds number the flow follows the contour of the wall. However, a tendency to separation can also be observed. As the Reynolds number increases separation bubbles begin to appear and grow at the upstream corner of the top wall and downstream corner of the bottom wall. At $Re = 719$ large circulation zones have also been developed in the vicinity of the lower part of the top wall. On the upper horizontal part of the bottom wall a weak recirculation zone is formed at the highest Reynolds numbers. As the Reynolds number is further increased to 1200, the sizes of these circulation zones are increased somewhat. The downstream oblique part of the top wall and the lower left part of the bottom wall experience attached flow. Once the recirculation zones are well established, there is a separation shear layer which divides the flow into two parts, the separated flow regions within which the fluid circulates as indicated in the Figures and the main flow region where the streamlines tend to be parallel to each other. The shear layer re-attaches to the surface behind the separated region. The presence of the separation bubbles and the re-attachment influences the heat transfer from the duct walls and affects the pressure drop.

In the case of the duct with $\phi = 15°$, only a tiny separation bubble appeared at the left corner of the top wall at high Reynolds number (≈ 1200), otherwise the flow follows the contour of the wall.

Pressure drop

Representative results for the fully developed per-cycle pressure drop ratio, (14), vs. Reynolds number with module aspect ratio as curve parameter are presented in *Figure 4* for both inclination angles 15° and 45°. The highest pressure drop is obtained for $H/L = 1/5$ and $\phi = 45°$. For an inclination angle of 45° the pressure drop increases by decreasing the module aspect ratio whereas for an inclination angle of 15° the module aspect ratio has only a small effect on the pressure

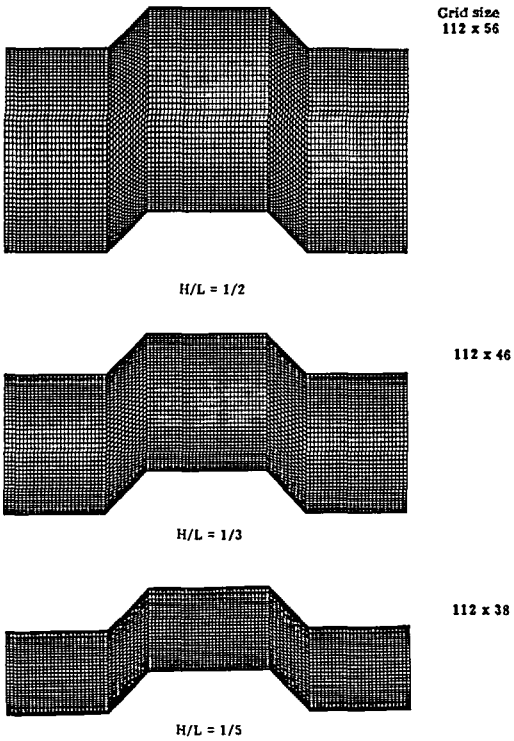

Figure 2 Solution domain and computational grid for $\phi = 45°$ and different H/L

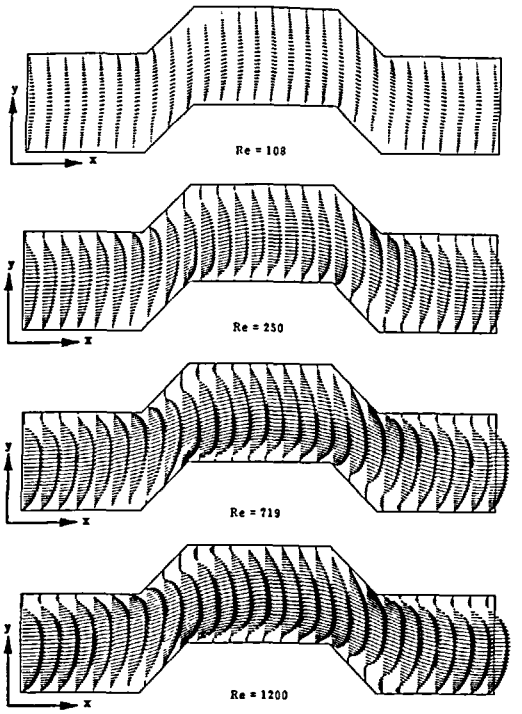

Figure 3 Velocity vectors for $H/L = 1/5$ and $\phi = 45°$

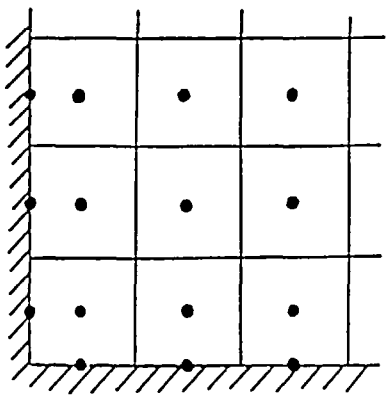

Figure 2b Principal sketch of the employed grid close to walls

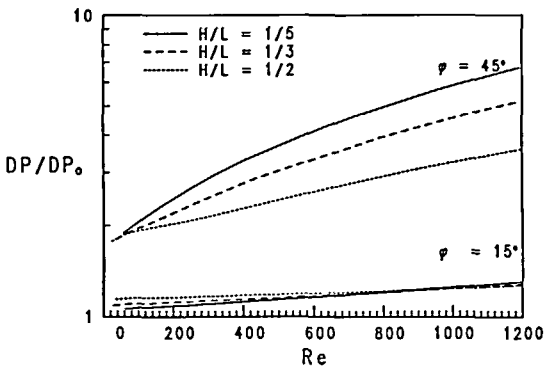

Figure 4 Pressure drop ratio vs. Reynolds number

drop. Irrespective of the inclination angles, the pressure drop increases with increasing Reynolds number. However, this increase is very moderate in the case of $\phi = 15°$. For $\phi = 15°$, the curves show a cross-over at $Re \approx 900$.

Overall Nusselt number

Fully developed per-cycle overall Nusselt number, (19), have been determined as function of

Reynolds number with inclination angle and module aspect ratio as parameters. The results are plotted in *Figure 5*. As is shown in the Figures, the overall Nusselt number for the duct with module aspect ratio 1/5 is increasing monotonically with increasing Reynolds number. On the other hand, a strong overshoot can be observed at low Reynolds number (≈ 100) for $H/L = 1/3$ and 1/2 in both cases of inclination angles. For Reynolds number above $Re \approx 300$, the increase in Nusselt number for all three cases of module aspect ratios takes a similar trend. It is also found that at higher Reynolds numbers ($\geqslant 800$, $\phi = 45°$; $\geqslant 600$, $\phi = 15°$) the Nusselt number increases with decreasing module aspect ratio.

The over-shoot of the Nusselt number for the cases of $H/L = 1/3$ and 1/2 at low Reynolds number was taken into serious consideration by among other things employing different grid sizes and studying the results which are presented in *Table 2*. The value of the average Nusselt number remained unchanged as different grid sizes were tested. The existence of the over-shoots for $H/L = 1/3$ and $H/L = 1/2$ is surprising. The pressure drop distributions, *Figure 3*, are not showing any peculiar dependence on Reynolds number. From the streamlines and isotherm plots at Reynolds number around 100 it is not possible to figure out any physical interpretation for this behaviour. Earlier investigations on other duct geometries[6,10] reveal also peculiar behaviour at low *Re*, which may be attributed to the certain dimensions under consideration.

It is worthwhile to note that the Nusselt number for a parallel plate is 7.54 which was also computed in this work. By corrugating the channel walls a substantial increase in the heat transfer from the fluid to the walls, particularly at high inclination angles, is achieved.

Local Nusselt number

Distributions of the local Nusselt number are plotted in *Figures 6a, 6b* and *6c*. In *Figure 6a* the local Nusselt number distribution for $\phi = 45°$ and $H/L = 1/5$ is presented for three different Reynolds numbers. In *Figure 6b*, *Nu* distributions for $Re = 250$ and $H/L = 1/5$ are plotted for two different inclination angles. In *Figure 6c* the local Nusselt numbers distributions for $Re = 100$ and $\phi = 45°$ are shown for three different module aspect ratios. As seen from these Figures the local Nusselt number at the top and the bottom walls have a similar pattern of development. The duct can be divided into five different sections. Section one is the upstream horizontal section, section two is the upstream oblique section, section three is the middle horizontal section, section four is the downstream oblique section and section five is the downstream horizontal section. At the top wall of the first section the local Nusselt number increases until we enter the second section. In this section at the oblique wall of the top wall, the Nusselt number decreases sharply until we approach section three. This latter section by itself consists of two parts. The

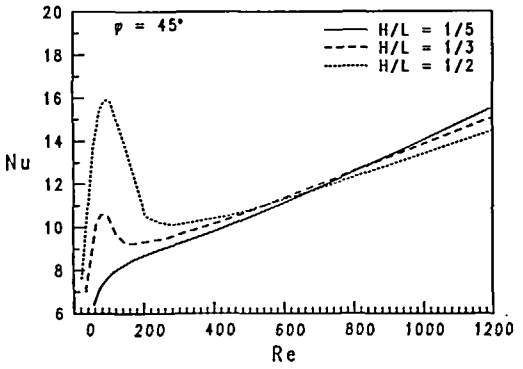

Figure 5a Overall Nusselt number vs. Reynolds number for $\phi = 45°$

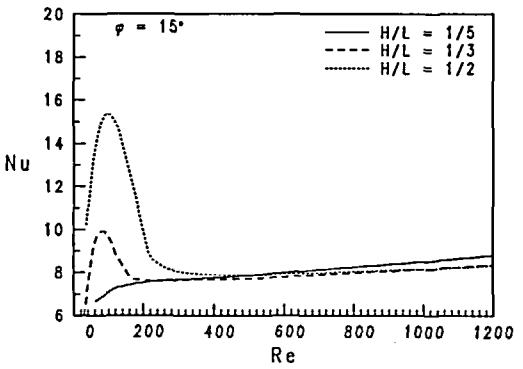

Figure 5b Overall Nusselt number vs. Reynolds number for $\phi = 15°$

length of the first part is 1/3 of this section and the remaining length is the second part. In the first part the local Nusselt number increases. This increase is stronger for higher Reynolds number, see *Figure 6a*, and for higher inclination angle, see *Figure 6b*, and for smaller module aspect ratio, see *Figure 6c*. In the second part of the third section the local Nusselt number decreases until we enter the fourth section. At the downstream oblique wall the local *Nu* increases sharply to its maximum value which lies at the interface of the fourth and fifth sections. Right at the beginning of the fifth section the local *Nu* falls sharply and continues to decrease at a moderate rate. In this section, contrary to the first and third section, the value of the local *Nu* is lower for higher Reynolds number and higher inclination angle and for smaller module aspect ratio.

We now turn our attention to the bottom wall. In the first section the local Nusselt number decreases moderately until we enter the second section. Here the local *Nu* increases very sharply to its maximum value and falls very rapidly again in the beginning of the third section. In the second part of the third section the local *Nu* starts to increase to another maximum value. At the oblique wall of the fourth section, *Nu* decreases sharply until we approach the fifth section where *Nu* increases over the separated region and starts to decrease thereafter.

The effect of the different parameters *Re*, ϕ, and H/L can be seen in all three Figures. The significant effect of the inclination angle on the local Nusselt number distribution can be observed in *Figure 6b*.

Let us now focus our attention to the physical interpretation of the results. In the separated flow regions, the recirculating fluid behaves as a conveyor carrying heat from the core to the wall. The recirculating fluid itself should be divided into two parts, a downstream and an upstream part. In the downstream part of the recirculating fluid, the heat is conveyed from the separated layer to the wall causing a high temperature difference at the wall and thus an increase

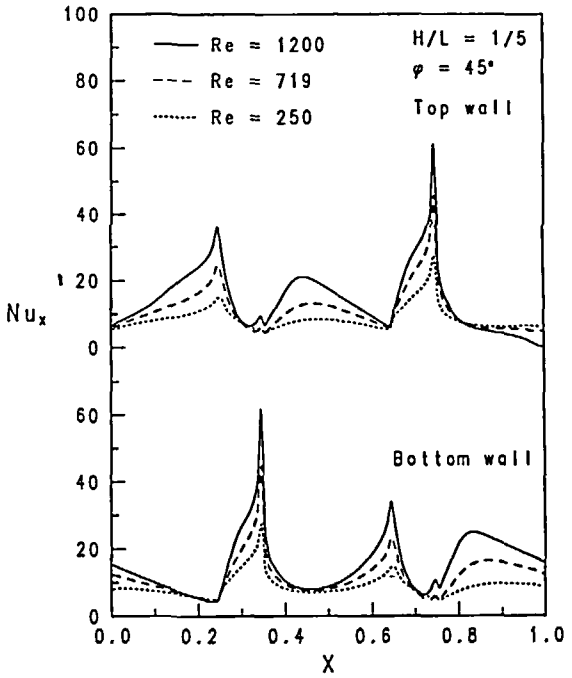

Figure 6a Local Nusselt number distributions for $H/L = 1/5$ and $\phi = 45°$

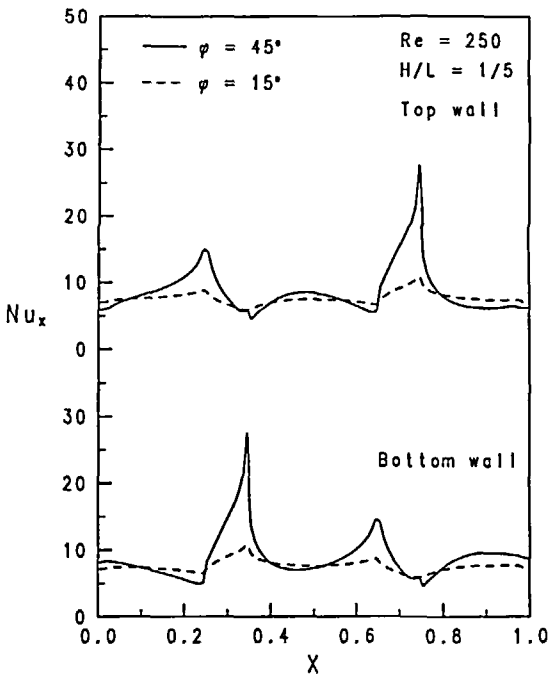

Figure 6b Local Nusselt number distributions for $H/L = 1/5$ and $Re = 250$

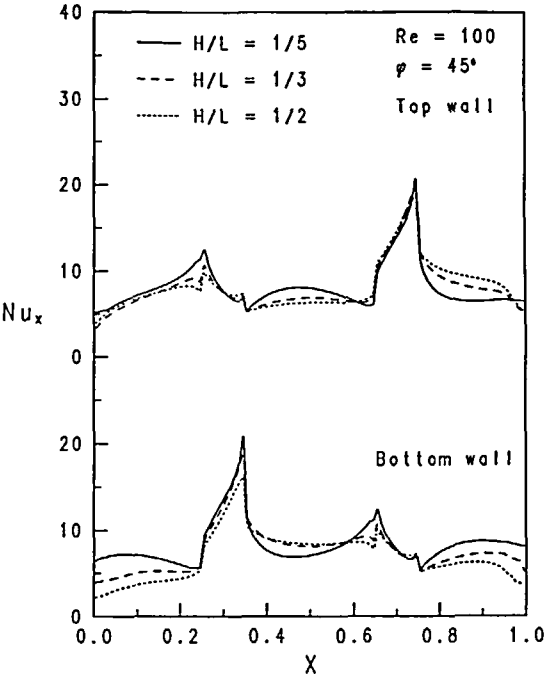

Figure 6c Local Nusselt number distributions for $Re = 100$ and $\phi = 45°$

in the local Nusselt number. The temperature gradient between the wall and the upstream part of the recirculation becomes smaller and therefore the heat transfer between the wall and the fluid is reduced which causes reduction in the local Nusselt number. In re-attached regions the heat is directly convected to the wall by the mainflow. Thus the steepness of the temperature gradient is increased and we experience increase in the local Nusselt number.

A double-peak in the distributions of the local Nusselt number can be observed at the upstream corner of the top wall and downstream corner of the bottom wall. These peaks were also investigated further. Two different tests were carried out. In the first test a high concentration of nodes at both these corners were employed and in the second test the corners were slightly rounded. The results from these two cases were compared with the results obtained from the uniform grid. No changes could be detected. The peaks take place right at the middle of the corresponding recirculation zones. The changes from orthogonal to non-orthogonal coordinates may affect the results locally. However, various distributions and sizes of the control volumes at the positions of changing the coordinate lines had a negligible influence on the calculated results.

CONCLUSIONS

The fully developed periodic heat transfer and fluid flow characteristics for laminar flow through streamwise-periodic corrugated ducts of various geometrical dimensions were obtained by employment of a finite-difference method in complex geometries which utilizes colocated variables and Cartesian velocities. Enhancement in the average Nusselt number compared with a parallel plate duct was found in all cases. This enhancement was very high at low Reynolds number (≈ 100) for two of the module aspect ratios. Otherwise an increase in Nusselt number was

obtained as Reynolds number increased. This increase in Nusselt number was very moderate in the duct with an inclination angle $\phi = 15°$. However, the gain in heat transfer is accompanied by a pressure drop penalty which is very large in the case of the duct with module aspect ratio 1/5 and inclination angle 45°. At very low Reynolds number, only the through flow can be observed in the duct with $\phi = 45°$ whereas at higher Reynolds number separation bubbles and recirculation zones are observed. However, in the duct with $\phi = 15°$ a small separation bubble appears only at high Reynolds number (≈ 1200). The temperature gradients at the wall become steeper as the Reynolds number is increased which causes an increase in the local Nusselt number.

ACKNOWLEDGEMENT

The financial support from the National Swedish Board for Technical Development (STU) is gratefully acknowledged.

REFERENCES

1 Shah, R. K. and Bhatti, M. S. Laminar convective heat transfer in ducts, in *Handbook of Single-Phase Convective Heat Transfer*, (Eds. S. Kakac, R. K. Shah and W. Aung), Wiley-Interscience, New York (1987)
2 Webb, R. L. Enhancement of single phase heat transfer, in *Handbook of Single-Phase Convective Heat Transfer*, (Eds. S. Kakac, R. K. Shah and W. Aung), Wiley-Interscience, New York (1987)
3 Patankar, S. V., Liu, C. H. and Sparrow, E. M. Fully developed flow and heat transfer in ducts having streamwise-periodic variations of cross-sectional area, *J. Heat Transfer*, **99**, 180–186 (1977)
4 Sparrow, E. M. and Prata, A. T. Numerical solution for laminar flow and heat transfer in a periodically converging-diverging tube with experimental confirmation, *Num. Heat Transfer*, **6**, 441–461 (1983)
5 Prata, A. T. and Sparrow, E. M. Heat transfer and fluid flow characteristics for an annulus of periodically varying cross-section, *Num. Heat Transfer*, **7**, 285–304 (1984)
6 Rowley, G. L. and Patankar, S. V. Analysis of laminar flow and heat transfer in tubes with internal circumferential fins, *Int. J. Heat Mass Transfer*, **27**, 553–560 (1984)
7 Faghri, M. and Asako, Y. Numerical determination of heat transfer and pressure drop characteristics for converging-diverging flow channel, *ASME Winter A. Meet, Paper no. 84-WA-HT-12* (1984)
8 Asako, Y. and Faghri, M. Heat transfer and fluid flow analysis for an array of interrupted plates, positioned obliquely to the flow direction, in *Proc. 8th Int. Heat Transfer Conf.*, **2**, 421–427 (1986)
9 Webb, B. W. and Ramadhyani, S. Conjugate heat transfer in a channel with staggered ribs, *Int. J. Heat Mass Transfer*, **28**, 1679–1687 (1985)
10 Sunden, B. and Trollheden, S. Periodic laminar flow and heat transfer in a corrugated two-dimensional channel, *Int. Commun. Heat Mass Transfer*, **16**, 215–225 (1989)
11 Farhanieh, B. and Sunden, B. Numerical investigation of periodic laminar heat transfer and fluid flow characteristics in parallel plate ducts with streamwise-periodic cavities, *Int. J. Num. Meth. Heat Fluid Flow*, **1**, 143–157 (1991)
12 Davidson, L. and Farhanieh, B. A finite-volume code employing colocated variable arrangement and cartesian velocity components for computation of heat and mass transfer in complex three-dimensional geometries, *Publication no. 91/14*, Dept. of Thermo- and Fluid Dynamics, Chalmers University of Technology, Göteborg (1991)
13 Farhanieh, B. and Sunden, B. Three-dimensional laminar flow and heat transfer in entrance region of trapezoidal ducts, *Int. J. Num. Meth. Fluids*, (13), 537–556 (1991)
14 White, F. M. *Fluid Mechanics*, Second Edn, McGraw-Hill, Singapore (1987)
15 Eckert, E. R. G. and Drake, R. M. *Analysis of Heat and Mass Transfer*, Hemisphere, New York (1987)
16 Herman, C. V. and Mayinger, F. Interferometric study of heat transfer in a grooved geometry, in *Experimental Heat Transfer, Fluid Mechanics, and Thermodynamics*, (Eds. J. F. Keffer, R. K. Shah and E. N. Ganic), Elsevier, New York, pp. 522–529 (1991)